applied sciences

MDPI

Article

Optimal Design of Wearable Micro Thermoelectric Generator Working in a Height-Confined Space

Kechen Tang, Dongwang Yang *, Yubing Xing, Jiang Wang, Kai Hu, Yonggao Yan *, Qingjie Zhang and Xinfeng Tang *

State Key Laboratory of Advanced Technology for Materials Synthesis and Processing, Wuhan University of Technology, Wuhan 430070, China; tangkechen@whut.edu.cn (K.T.)

* Correspondence: ydongwang@whut.edu.cn (D.Y.); yanyonggao@whut.edu.cn (Y.Y.); tangxf@whut.edu.cn (X.T.)

Abstract: With the increasing development of self-powered wearable electronic devices, there is a growing interest in thermoelectric generators (TEGs). To achieve more comprehensive and reliable functionality of wearable devices, improving the power generation performance of thermoelectric devices will be the key. It has been shown that integrating a heat sink at the cold end of the TEG increases the effective temperature difference and, thus, maximizes the power output of the thermoelectric device. However, the space left for the power supply is often limited. How to optimize the integrated system of micro-thermoelectric generators and heat sinks in a height-confined space has become the key. In this study, we have established a corresponding model using a numerical calculation method, systematically studied the influence of TEG geometric size on the number of fins and fin height, and determined the optimal number of fins for the highest equivalent convective heat transfer coefficient corresponding to different fin heights. We also conducted the co-design of TEG and fin topological structure to study the effects of the ratio of leg height to fin height (l/H), the width of legs (w), and the number of thermoelectric leg pairs (N) on the maximum output power density per unit area (P_{m1}) and the maximum output power density per unit mass (P_{m2}) of the device. When $N = 16$, $w = 0.3$ mm, $l/H = 2.5$ (that is, $l = 3.57$ mm, $H = 1.43$ mm), and P_{m1} reaches the maximum value of 30.5 μW/cm^2; When $N = 2$, $l/H = 0.25$ and $w = 0.3$ mm, and P_{m2} reaches a maximum value of 5.12 mW/g. The measured values of the open-circuit voltages of fabricated micro-TEGs with different thermoelectric leg heights ($l = 0.49$ mm, $l = 1.38$ mm, and $l = 1.88$ mm) are basically consistent with the simulated values. When $N = 2$, $l = 0.49$ mm, $H = 3.74$ mm, and $w = 0.85$ mm, and P_{m2} reaches 0.44 mW/g. The results provide insights into the optimal design of wearable micro thermoelectric generator working in a height-confined space and highlight the importance of co-designing TEGs and fin topological structures for optimizing their performance.

Keywords: micro thermoelectric generator; wearable device; finite element simulation; heat sink; power density

Citation: Tang, K.; Yang, D.; Xing, Y.; Wang, J.; Hu, K.; Yan, Y.; Zhang, Q.; Tang, X. Optimal Design of Wearable Micro Thermoelectric Generator Working in a Height-Confined Space. *Appl. Sci.* **2023**, *13*, 6156. https://doi.org/10.3390/app13106156

Academic Editors: Norhisam Bin Misron and Chockalingam Aravind Vaithilingam

Received: 20 April 2023
Revised: 11 May 2023
Accepted: 15 May 2023
Published: 17 May 2023

1. Introduction

Wearable micro-electronic devices have become increasingly popular across various fields, including health monitoring [1,2], implantable medical devices [3–5], Internet of Things [6,7], and intelligent sensors [8–10]. However, a significant limitation of traditional wearable devices is their limited battery capacity which necessitates frequent recharging. This may harm the product performance and user experience of micro-electronic systems. To overcome this challenge, self-powered technology has emerged as a promising solution. By harnessing energy from the environment, such as light [11–13], heat [14–16], and vibration [17,18], self-powered technology can provide a continuous energy source for micro-electronic devices, thereby eliminating the need for external power supplies. This is particularly advantageous for wearable devices, which require a reliable and convenient energy source to sustain their operation.

Thermoelectric generators (TEGs) enable the direct conversion of thermal energy and electrical energy by utilizing carrier motion in solid materials. The advantages of TEGs, including compactness, stability, silence, absence of moving parts, and environmental friendliness, have made them an attractive option for a wide range of applications [19–21]. In particular, there is a growing interest in utilizing TEGs for developing self-powered wearable devices [22–24]. Recent research has demonstrated that TEGs are capable of providing sufficient power to operate different body sensors. This breakthrough has opened up new possibilities for developing wearable devices that are self-sufficient and do not require external power sources. TEGs can be integrated into a range of wearable devices, including smartwatches, fitness trackers, and medical monitors, to provide a reliable and continuous source of power. Wang et al. designed a wearable thermoelectric generator with a flexible printed circuit board (FPCB) as its substrate. The results show that the TEG can provide power for a three-axis micro accelerometer to detect body motion when the temperature difference is 18 K [25]. Torfs et al. have implemented a wearable wireless dual-channel EEG system driven entirely by human heat that generates more than 2 mW of power at 23 °C [26]. Mohsen et al. has developed a photoelectric-thermoelectric hybrid system to power medical sensors, which can be used to monitor body temperature, heartbeat, and blood oxygen saturation in real time [27].

In order to realize the full potential of wearable devices, it is crucial to improve the power generation performance of TEGs. This requires maintaining a sufficient temperature difference to achieve high open-circuit voltage and power density in TEGs. One effective way to achieve this temperature difference is to install a heat dissipation device at the cold end of the TEG. This can enhance the effective temperature difference, allowing for maximum power output [28–32]. A fin radiator is a common semi-active heat dissipation device with a simple structure and low price. Chen et al. considered a thermoelectric module without fins as well as with plate fins and square pin fins. The results show that the installation of both plate fins and square pin fins can significantly enhance waste heat collection [33]. Garud et al. studied six different fin structures and compared their temperature distribution, pressure drop, net power output, overall efficiency, and stress. The heat exchanger with an oblique fin and vertical fin has higher net power output and overall efficiency [34]. Abdelhadi et al. compared the effects of fin material and geometry on heat dissipation capacity. It reveals that the shape and design of the heat sink is very important for transporting heat from the top to the bottom, but the complex design brings high costs and is difficult to industrialize [35]. Kim et al. studied the optimal number and thickness of fins for thermoelectric power generation and proposed a modified thermal resistance equation to predict the heat transfer characteristics of plate fins used for heat absorption in TEGs [36]. Quan et al. evaluated the influence of the internal topology and fin parameters on the heat transfer and power output of the TEG system. It reveals that increasing the fin length and width is beneficial to the maximum output power. Reducing the fin spacing helps to increase the maximum power of the TEG system [37].

In wearable electronic devices, the space left for power is often limited (as shown in Figure 1). When the total height of the TE leg and heat dissipation fins is fixed, it is critical to optimize the topology of TEG system for maximum power output. Numerical simulation is a convenient, economical, and effective way. In this study, we use finite element numerical simulation to cooperatively design the topology of thermoelectric generator and fins. The inherent non-linear temperature dependence of TE materials and related effects, including Seebeck, Peltier, Thomson, and irreversible Joule heating are all considered. The effects of the ratio of TE leg height to fin height (l/H), TE leg width (w), and the number of leg pairs (N) on the maximum output power density of the device are investigated. Finally, the corresponding TEG is compiled, and the simulation results are verified.

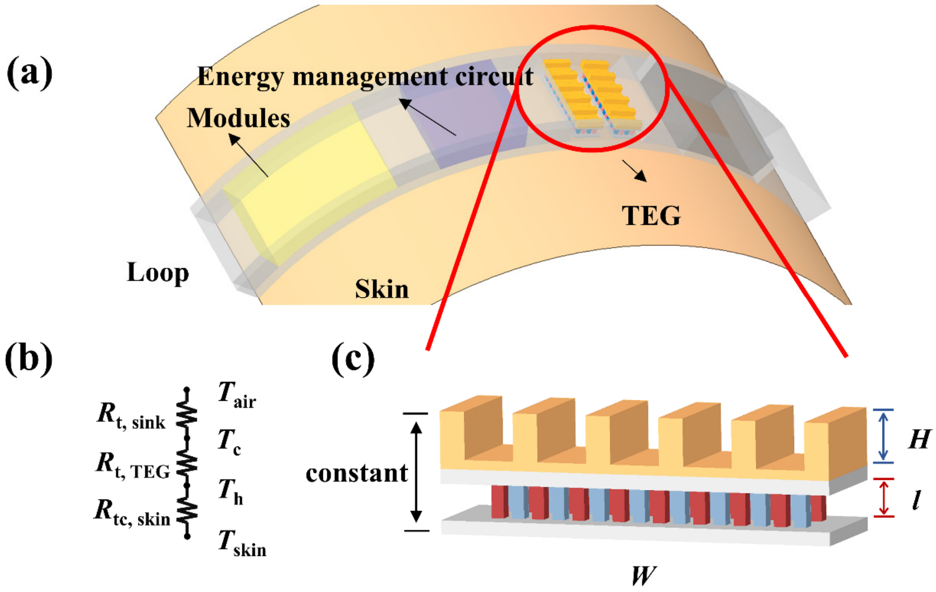

Figure 1. (**a**) The structure of wearable TEG in a height-confined space; (**b**) schematic of thermal resistance from skin to environment; (**c**) integrated design of TEG and heat dissipation fin with fixed overall height.

2. Experimental

2.1. Simulation Modeling

In this work, the finite element method employed in the ANSYS Workbench platform was used to study the distribution of temperature, the open-circuit voltage (V_{oc}), and the maximum output power (P_{max}) of TEGs with various parameters.

Ignoring thermal losses, when an external load resistor is connected to the TE module, the output power is expressed as

$$P = \left(\frac{V_{oc}}{R_L + R_{in}}\right)^2 \times R_L \tag{1}$$

where R_L is the external load resistance and R_{in} is the TE module's internal resistance.

2.2. Governing Equations for Thermoelectric Analysis

The governing equation of heat flow in a TEG module can be expressed as [38]

$$\rho C \frac{\partial T}{\partial t} + \nabla \cdot \boldsymbol{q} = \dot{q}, \tag{2}$$

where C is the specific heat capacity, ρ is the density, T is absolute temperature, $\boldsymbol{q}$ is the heat flux vector, and $\dot{q}$ is the heat generation rate per unit volume.

And the continuity equation of electric charge can be written as [38]

$$\nabla \cdot \left(\boldsymbol{J} + \frac{\partial \boldsymbol{D}}{\partial t}\right) = 0, \tag{3}$$

where $\boldsymbol{J}$ is the electric current density vector, and $\boldsymbol{D}$ is the electric flux density vector.

Equations (1) and (2) are coupled by the set of thermoelectric constitutive equations as follows [39]:

$$\boldsymbol{q} = T[\alpha] \cdot \boldsymbol{J} - [\kappa] \cdot \nabla T, \tag{4}$$

$$\boldsymbol{J} = [\sigma] \cdot (\boldsymbol{E} - [\alpha] \cdot \nabla T), \tag{5}$$

where $[\alpha]$ is the Seebeck coefficient matrix, $[\kappa]$ is the thermal conductivity matrix, and $[\sigma]$ is the electrical conductivity matrix. The electric field intensity vector $\boldsymbol{E}$ is irrotational ($\nabla \times \boldsymbol{E} = 0$), and can be derived from the electric scalar potential:

$$\boldsymbol{E} = -\nabla \varphi. \tag{6}$$

The equation for a dielectric medium can be expressed as

$$D = [\varepsilon] \cdot \boldsymbol{E}, \tag{7}$$

where $[\varepsilon]$ is the dielectric permittivity matrix.

Substituting Equations (3) and (4) into Equations (1) and (2) produces a system of coupled equations of thermoelectricity:

$$\rho C \frac{\partial T}{\partial t} + \nabla \cdot (T[\alpha] \cdot \boldsymbol{J}) - \nabla \cdot ([\kappa] \cdot \nabla T) = \dot{q}, \tag{8}$$

$$\nabla \cdot \left([\varepsilon] \cdot \nabla \frac{\partial \varphi}{\partial t} \right) + \nabla \cdot ([\sigma] \cdot [\alpha] \cdot \nabla T) + \nabla \cdot ([\sigma] \cdot \nabla \varphi) = 0, \tag{9}$$

where $\dot{q}$ includes the electric power $\boldsymbol{J} \cdot \boldsymbol{E}$ spent on Joule heating and on work against the Seebeck field $[\alpha]\ \nabla T$.

If the simulation is based on the steady-state model and materials properties of all components are considered to be isotropic, Equations (7) and (8) can be simplified as

$$\nabla \cdot (T \alpha \boldsymbol{J}) - \nabla \cdot (\kappa \nabla T) = \dot{q}, \tag{10}$$

$$\nabla \cdot (\sigma \alpha \nabla T) + \nabla \cdot (\sigma \nabla \varphi) = 0. \tag{11}$$

2.3. Discrete Calculation Process of Finned Heat Sink

The section diagram of the fin structure can be referred to the Figure 3a. The starting point for calculating the temperature is the bottom temperature (T_{base}) of the finned radiator base. The qualitative temperature (T) can be obtained by taking the average of the ambient temperature (T_{m}) and the bottom temperature of the finned radiator base, as expressed:

$$T = (T_{\mathrm{base}} + T_{\mathrm{m}})/2 \tag{12}$$

To determine whether natural convective heat transfer on the uncovered upper surface of the fin radiator base is limited, the ratio of fin spacing (S) to fin height (H) is used as a criterion [40].

When $S/H \leq 0.28$, Incropera et al. [41] proposed to use Gr_{base} as a criterion to for calculating the convective heat transfer coefficient h across different ranges of Gr:

$$\begin{gathered} Nu_{base} = 1,\ Gr_{base} \leq 2430 \\ Nu_{base} = 0.212 \times (Gr_{base} \times \mathrm{Pr}_{base})^{0.25},\ 1.0 \times 10^4 \leq Gr_{base} \leq 4.6 \times 10^5, \\ Nu_{base} = 0.061 \times (Gr_{base} \times \mathrm{Pr}_{base})^{1/3}, Gr_{base} > 4.6 \times 10^5, \end{gathered} \tag{13}$$

$$Gr_{base} = \frac{\mathrm{g} \times \beta \times (T_{\mathrm{base}} - T_{\mathrm{m}}) \times H^3}{\nu^2}, \tag{14}$$

$$h_{base} = \frac{Nu_{base} \times k_{\mathrm{air}}}{H} \tag{15}$$

where Nu_{base}, Gr_{base}, Pr_{base}, k_{air}, β, ν represent the Nusselt number, Grashof number, Prandtl number, thermal conductivity, volumetric expansion coefficient, and kinematic viscosity of air at qualitative temperature, respectively. The characteristic scale is taken as the fin height H and g is the gravitational acceleration which is 9.8 $\mathrm{m/s^2}$.

When $S/H > 0.28$, Incropera et al. [41] used Rayleigh number $Ra_{base} = Gr_{base} \times \mathrm{Pr}_{base}$ as a criterion to obtain convective heat transfer coefficient in different ranges of Ra:

$$\begin{aligned} Nu_{base} &= 1,\ Ra_{base} < 2\times10^4 \\ Nu_{base} &= 0.54\times(Gr_{base}\times\mathrm{Pr}_{base})^{0.25},\ 1.0\times10^5 \le Ra_{base} \le 2\times10^7, \\ Nu_{base} &= 0.14\times(Gr_{base}\times\mathrm{Pr}_{base})^{1/3},\ 2\times10^7 \le Ra_{base} \le 3\times10^{10}, \end{aligned} \tag{16}$$

$$Gr_{base} = \frac{g\times\beta\times(T_{\mathrm{base}}-T_{\mathrm{m}})\times {l_{base}}^3}{\nu^2}, \tag{17}$$

$$h_{base} = \frac{Nu_{base}\times k_{\mathrm{air}}}{l_{base}} \tag{18}$$

$$l_{base} = \frac{S\times L}{2\times(S+L)} \tag{19}$$

where l_{base} is the characteristic length, and S and L are the spacing and length of the fins.

To calculate convective heat transfer in the middle of the fin, Bar-Cohen et al. [42] extended the Elenbass empirical correlation equation and proposed the following calculation process:

$$Nu_{fin} = \left(\frac{576}{\left(\eta_{fin}\times Ra_{fin}\right)^2} + \frac{2.873}{\left(\eta_{fin}\times Ra_{fin}\right)^{0.5}}\right)^{-0.5}, \tag{20}$$

$$Ra_{fin} = \frac{g\times\beta\times(T_{\mathrm{base}}-T_{\mathrm{m}})\times\mathrm{Pr}_{base}\times S^4}{L\times\nu^2}, \tag{21}$$

$$\eta_{fin} = \frac{\tan\mathrm{h}(m\times H^{\sim})}{m\times H^{\sim}}, \tag{22}$$

$$m = \sqrt{\left(h_{fin}\times2\times(L+t)\right)/(k_{\mathrm{fin}}\times L\times t)} \tag{23}$$

$$H^{\sim} = H + t/2 \tag{24}$$

$$h_{fin} = \frac{Nu_{fin}\times k_{\mathrm{air}}}{S} \tag{25}$$

where η_{fin} is the fin efficiency, the characteristic scale is taken as the fin spacing S, t is the thickness of a single fin, and k_{fin} is the thermal conductivity of the fin. To improve the accuracy of convective heat transfer coefficient calculation in fin structures, a closed−loop calculation program is proposed, as detailed in Method in Supplementary Material.

The convection heat transfer mechanism of the end fins is relatively straightforward. Incropera et al. [41] provided a formula for convection heat transfer under varying Gr ranges, based on Gr_{edge} criterion:

$$\begin{aligned} Nu_{edge} &= 0.59\times\left(Gr_{edge}\times\mathrm{Pr}_{base}\right)^{0.25},\ 1.43\times10^4 \le Gr_{\mathrm{edge}} \le 3\times10^9, \\ Nu_{edge} &= 0.0292\times\left(Gr_{edge}\times\mathrm{Pr}_{base}\right)^{0.39},\ 3\times10^9 \le Gr_{\mathrm{edge}} \le 2\times10^{10}, \\ Nu_{edge} &= 0.11\times\left(Gr_{\mathrm{edge}}\times\mathrm{Pr}_{base}\right)^{1/3},\ Gr_{edge} > 2\times10^{10}, \end{aligned} \tag{26}$$

$$Gr_{\mathrm{edge}} = \frac{g\times\beta\times(T_{\mathrm{base}\times}-T_{\mathrm{m}})\times H^3}{\nu^2}, \tag{27}$$

$$h_{edge} = \frac{Nu_{edge} \times k_{\mathrm{m}}}{H} \tag{28}$$

Finally, the total heat dissipation Q of the radiator can be obtained as follows.

$$Q_{\mathrm{base}} = h_{\mathrm{base}\times}\ (n-1) \times S \times L \times (T_{\mathrm{base}} - T_{\mathrm{m}}\ ), \tag{29}$$

$$Q_{\mathrm{fin}} = h_{\mathrm{fin}\times}\ (n-1) \times 2 \times H \times L \times (T_{\mathrm{base}} - T_{\mathrm{m}}\ ), \tag{30}$$

$$Q_{\mathrm{edge}} = h_{\mathrm{edge}\times}\ 2 \times H \times L \times (T_{\mathrm{base}} - T_{\mathrm{m}}\ ). \tag{31}$$

MATLAB was used to implement the logical calculations described above, and the program code is provided in the Supplementary Materials. In order to normalize the comparison of the heat dissipation capacity of the heat sink, the convective heat transfer coefficient per unit area (h_{a}) and the equivalent convective heat transfer coefficient of the fin (h_{eff}) were defined as follows.

$$h_{\mathrm{a}} = Q/(n-1) \times S \times L + 2n \times H \times (t+L) + n \times L \times t)/(T_{\mathrm{base}} - T_{\mathrm{m}}\ ), \tag{32}$$

$$h_{\mathrm{eff}} = Q/(W \times L)/(T_{\mathrm{base}} - T_{\mathrm{m}}\ ). \tag{33}$$

2.4. Boundary Conditions Setting

TEGs are usually packaged before being put into use. Therefore, their interior can be approximately regarded as being in a vacuum state. In order to simplify the calculation module and eliminate some unimportant factors, this study makes several basic assumptions for numerical simulation:

(1) Heat radiation influence near room temperature is ignored;
(2) Heat loss inside TEG caused by thermal convection can be ignored;
(3) Body surface temperature is set at 34 °C;
(4) Natural convection working environment of fin radiator is dry air at one standard atmospheric pressure and ambient temperature kept constant at 25 °C;
(5) Heat loss between heat sink and TEG cold end is negligible, i.e., temperature of fin baseplate equals that of cold end of TEG ($T_{\mathrm{c}} = T_{\mathrm{base}}$);
(6) Difference in fin surface convective heat transfer coefficient along fin height direction in fin group is small due to certain range of fin height and, thus, regarded as uniform for convenience of calculation;
(7) After heat dissipation reaches stability, the temperature gap of the lower surface of the fin radiator base is small and, thus, regarded as uniform.

2.5. Micro-TEG Fabricating

In this work, we have opted for the traditional π-type structure of thermoelectric generators (TEGs), consisting of p-type and n-type TE legs that are electrically connected in series and thermally connected in parallel. The heat sink features the most commonly used finned structure, fabricated from Cu material. In terms of the thermoelectric legs, we have utilized p-type $Bi_{0.4}Sb_{1.6}Te_3$ and n-type $Bi_2Se_{0.2}Te_{2.8}$ materials, and their properties are shown in Figure S1. The density of p- and n-type materials is 6.79 g/cm^3 and 7.82 g/cm^3, respectively. We have followed the micro-TEG fabrication process in Figure S2, which is consistent with our prior research work [43], to ensure the reliability and reproducibility of our experimental results.

3. Results and Discussion

3.1. Geometry Design of Finned Heat Sink

Based on the relevant formula regarding convective heat transfer of the fin, as detailed in Section 2.3, it can be inferred that the temperature difference between the fin base and the ambient surroundings ($\theta = T_{\text{base}} - T_{\text{m}}$) is a key factor that influences the heat dissipation capacity of the system, as illustrated in Figure 2a. To investigate the impact of various geometric parameters on θ, we have established models with different TE leg widths (w), leg heights (l), and the number of leg pairs (N). As shown in Figure 2b, when the number of thermoelectric legs remains constant, the temperature difference θ increases with the widening of w, while it decreases with the heightening of l. Additionally, when the number of TE leg pairs increases from 2 to 16, the temperature difference θ demonstrates a notable increase. Within the range of geometric dimensions of the corresponding device, θ ranges from approximately 3 to 8 K.

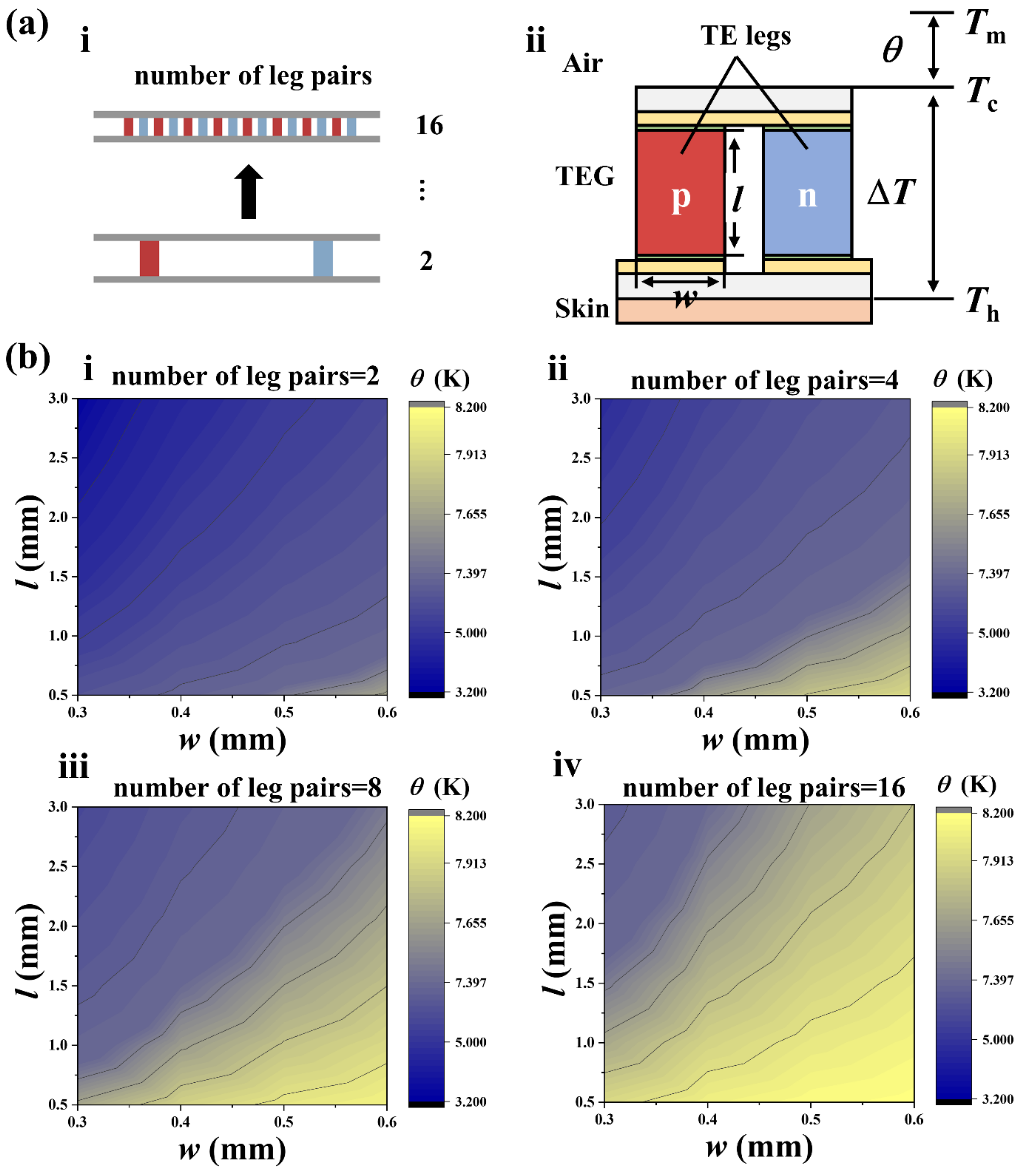

Figure 2. (**a**) Detailed drawing of corresponding parameters in TEG; (**b**) effect of TEG geometry parameter (leg width w, leg height l, number of leg pairs) on the temperature difference θ between fin base temperature and ambient temperature.

We conducted further analysis on the effect of the temperature difference θ on the heat dissipation capacity of the heat sink, as well as the equivalent convective heat transfer coefficient h_{eff} and convective heat transfer coefficient per unit area h_a, respectively (Figures 3a, S3 and S4). In order to normalize the results, we used the equivalent convective heat transfer coefficient h_{eff} as an indicator of the heat dissipation capacity of heat sinks with different geometric parameters. The difference of corresponding surface area between h_{eff} and h_a is represented by different colors in Figure 3a. We found that the h_{eff} of heat sinks with different fin numbers (n) (Figure 3b) and fin heights (H) (Figure 3c) are basically the same when θ increases from 4 K to 7 K. Therefore, the influence of the geometric size of the device on the heat dissipation capacity of the heat sink is negligible. In addition, we investigated the impact of the number of fins and fin heights on h_{eff} (Figure 3d,e). As presented in Figure 3d, with the increase of the number of fins, the h_{eff} initially increases to a certain value and then decreases sharply. The number of fins with a sudden drop decreases as the fin height increases. Moreover, Figure 3e shows that h_{eff} initially increased slowly with increasing fin height, sharply decreased at a certain point, and then increased slowly again. The above related laws are in line with the related theories of heat transfer. The fin height of the fin structure parameters of the fin radiator can effectively affect the natural convection heat transfer area, and the number of fins can effectively affect the air flow between the fins during natural convection heat dissipation [33].

Finally, we have conducted a comprehensive study on the impact of geometric parameters of fins on the temperature difference (θ) and heat dissipation capacity of a heat sink, as presented in our results. We have identified the optimal combination of geometric parameters of fins for achieving the highest heat dissipation capacity of the heat sink. Specifically, we have sorted out the optimal number of fins for the highest equivalent convective heat transfer coefficient (h_{eff}) corresponding to different fin heights, as illustrated in Figure 3f. Our findings reveal that the optimal number of fins gradually decreases as the fin height increases. These results provide valuable insights into the design and optimization of heat sinks and the impact of geometric parameters on the heat dissipation capacity.

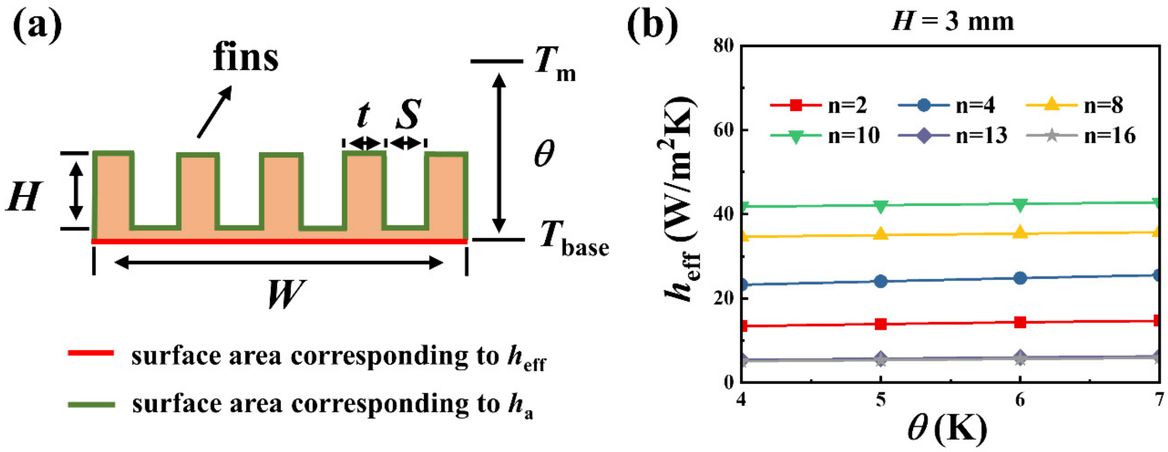

Figure 3. *Cont.*

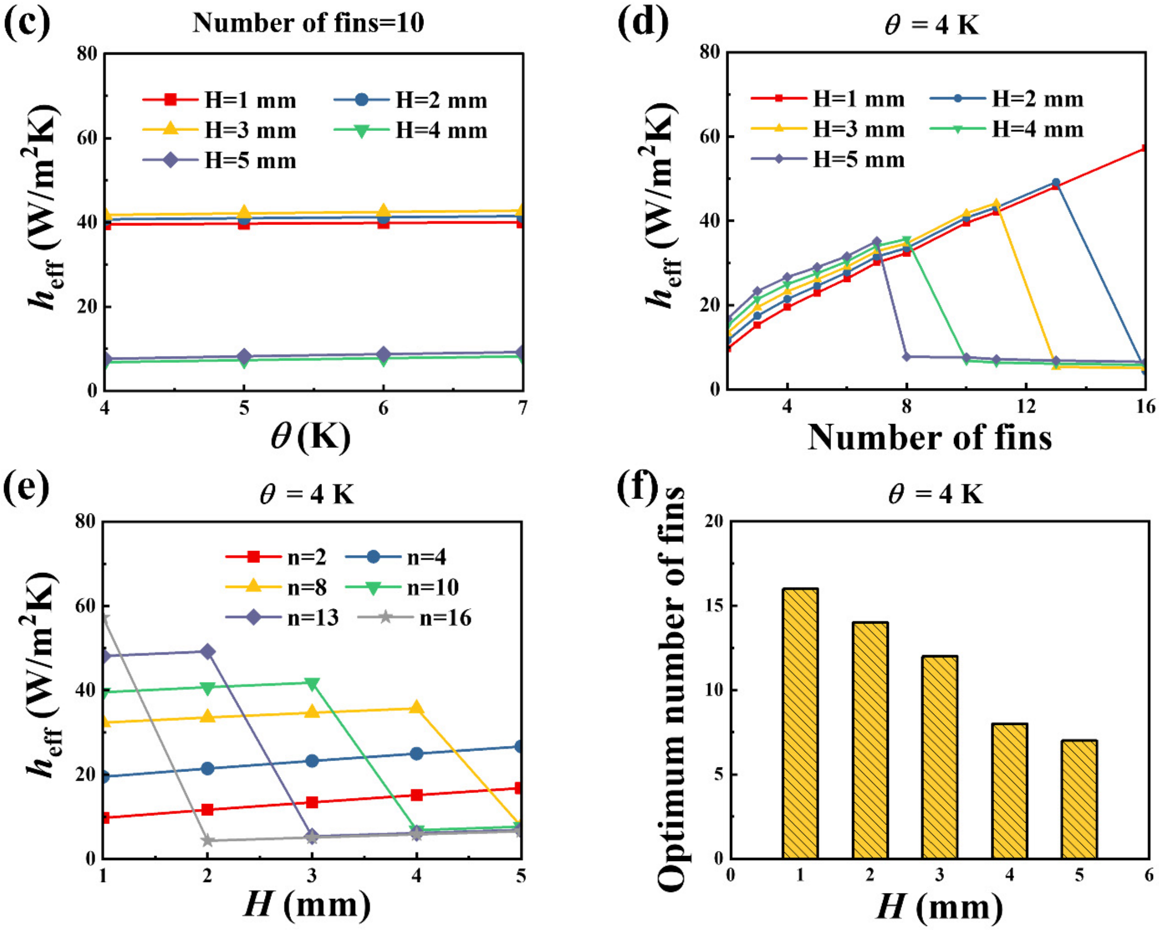

Figure 3. (**a**) Detailed drawing of corresponding parameters in finned radiator; (**b**–**e**) effect of temperature difference θ and geometric parameters of finned heat sink on the equivalent convective heat transfer coefficient h_{eff}; (**f**) relationship among the optimal number of fins, fin height H, and temperature difference θ.

3.2. Cooperative Optimization Design of the Overall Structure of TEG and Fin

After determining the optimal number of fins for the highest equivalent convective heat transfer coefficient, we conducted further studies to investigate the effects of various geometric parameters on the performance of the device. Specifically, we explored the impact of the ratio of leg height to fin height (l/H, where $l + H = 5$ mm), leg width (w), and number of leg pairs (N) on the maximum output power density per unit area (P_{m1}) (Figure 4) and the maximum output power density per unit mass (P_{m2}) (Figure 5) of the device, as well as the temperature difference at both ends of the device (ΔT) (Figure S5).

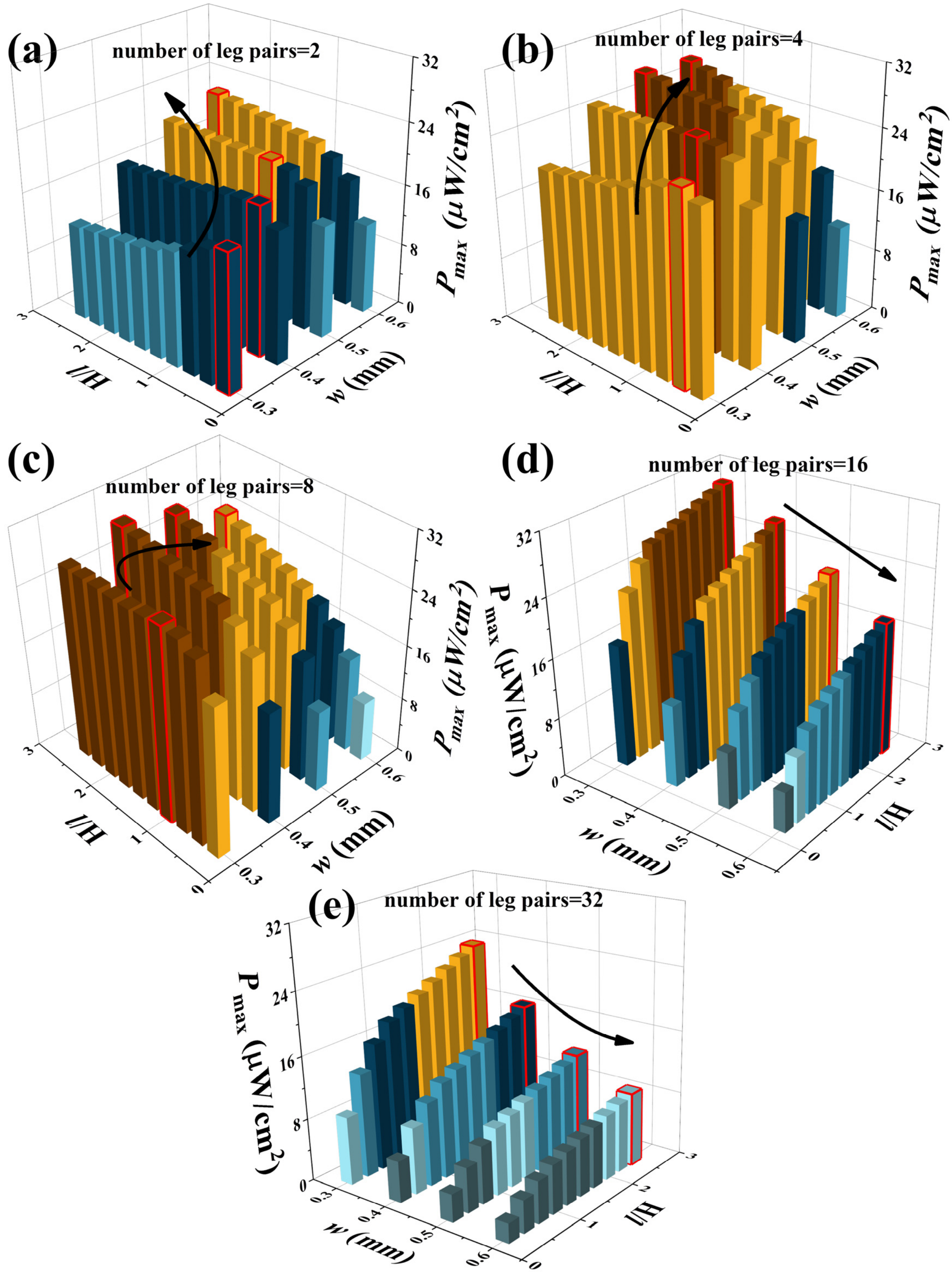

Figure 4. The relationship among the maximum power density per unit area (P_{m1}), leg width (w), and the ratio of leg height to fin height (l/H) with different number of leg pairs: (**a**) 2, (**b**) 4, (**c**) 8, (**d**) 16, and (**e**) 32.

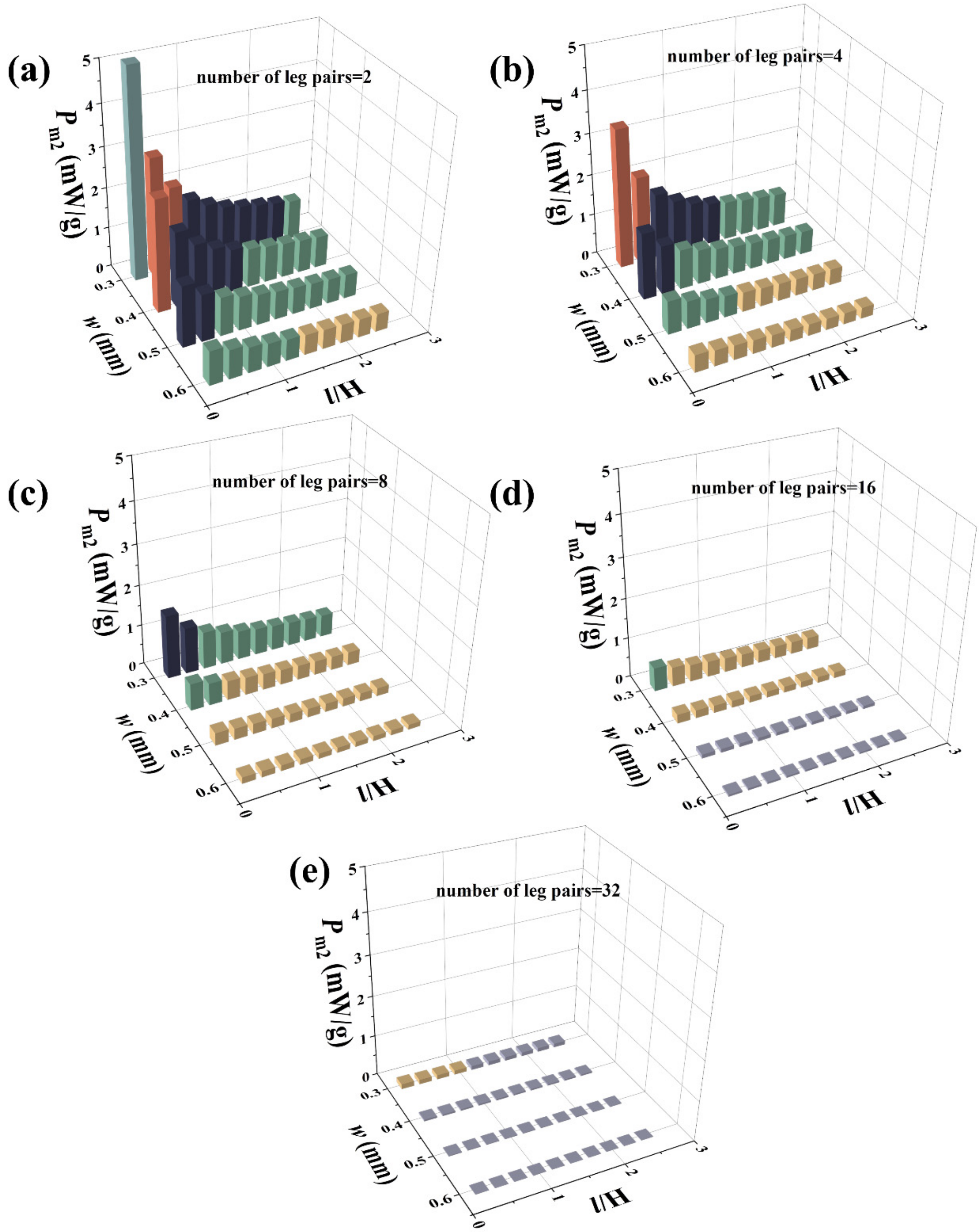

Figure 5. The relationship among the maximum power density of per unit mass (P_{m2}), leg width (w), and the ratio of leg height to fin height (l/H) with different number of leg pairs: (**a**) 2, (**b**) 4, (**c**) 8, (**d**) 16, and (**e**) 32.

Notably, we observed that the temperature difference (ΔT) decreased with an increase in both the number of leg pairs (N) and leg width (w), while it increased with an increase in l/H (Figure S5). The peak P_{m1} corresponding to different l/H and w is marked with red box in Figure 4. When N = 2, 4, the P_{m1} tends to obtain optimal value at both large l/H and w (Figure 4a,b); When N = 8, the P_{m1} first increases and then decreases with l/H as w = 0.3 mm, and the P_{m1} monotonously increases with l/H as w = 0.4~0.6 mm (Figure 4c); However, the trends are different when N = 16, 32. The P_{m1} increases monotonously with the increase of l/H, and decreases monotonously with the increase of w (Figure 4d,e). Specifically, when N = 16, w = 0.3 mm, the optimal l/H is 2.5 (i.e., l = 3.57 mm, H = 1.43 mm), and the corresponding P_{m1} reaches the highest value of 30.5 μW/cm^2. We compared the optimized simulation results with those previously reported in Table 1. As can be seen, radiators do greatly improve the performance of thermoelectric devices. Our optimized results are also at the forefront of research.

Table 1. Comparison between different TEG systems mentioned in the literature.

Authors	Output Power Density	Condition	TEG Location	Ref.
Wang et al.	0.3 μW/cm^2	No heat sink, ΔT = 5 K	Wrist	[25]
Kim et al.	2.28 μW/cm^2	No heat sink	Wrist	[44]
Shi et al.	4.07 μW/cm^2	No heat sink	Wrist	[45]
Leonov et al.	20 μW/cm^2	Very large heat sink	Wrist	[46]
Suarez et al.	20 μW/cm^2	Pin Radiator with no air flow	Wrist	[47]
Hong et al.	25.1 μW/cm^2	No heat sink, under cold condition	Forearm	[48]
Tang et al.	30.5 μW/cm^2	Finned Radiator, natural convection	Wrist	This Work

In addition to the maximum output power density per unit area (P_{m1}), we also evaluated the maximum output power density per unit mass (P_{m2}) of the device, which is a crucial factor in determining the price–performance ratio of the device. (Here, we mainly calculated the weight of TE material.) As can be seen in Figure 5, the P_{m2} of the device decreases monotonously with the increase of eg height-to-fin height ratio l/H, leg width w, and a number of leg pairs N. Specifically, the peak P_{m2} was observed when N = 2, l/H = 0.25 and w = 0.3 mm, reaching the highest value of 5.12 mW/g. The price–performance ratio of the device is an essential consideration for practical applications. Our results suggest that, from a cost perspective, it may be advantageous to choose a device with a lower l/H, narrower leg width, and a smaller number of leg pairs to achieve a higher P_{m2}. These findings provide important insights for the design and optimization of thermoelectric devices with improved efficiency and cost-effectiveness.

3.3. Verification of Simulation Results by Micro-TEG

In order to determine the credibility of the simulation results, several sets of controlled experiments were conducted. The existing thermoelectric leg size in the laboratory is w = 0.85 mm. To make it convenient and cost-effective, a device with N = 2 and heat sinks with different fin heights were designed. As shown in Figure 6, the measured values of the open-circuit voltages of three devices with different thermoelectric leg heights (l = 0.49 mm, l = 1.38 mm, l = 1.88 mm) are basically consistent with the simulated values under the condition of no heat sink and the heat sink with fins of corresponding height. With the addition of heat sinks, the performance of the device was significantly improved. When N = 2, l = 0.49 mm, H = 3.74 mm, w = 0.85 mm, and P_{m2} reaches 0.44 mW/g, which is 11 times higher than that before adding the heat sink. Since the heat loss between the radiator and the device is ignored in the simulation process, the calculated output power of the device is slightly higher than the measured value, while the error is within the allowable range. It can be seen that the simulation results are credible enough.

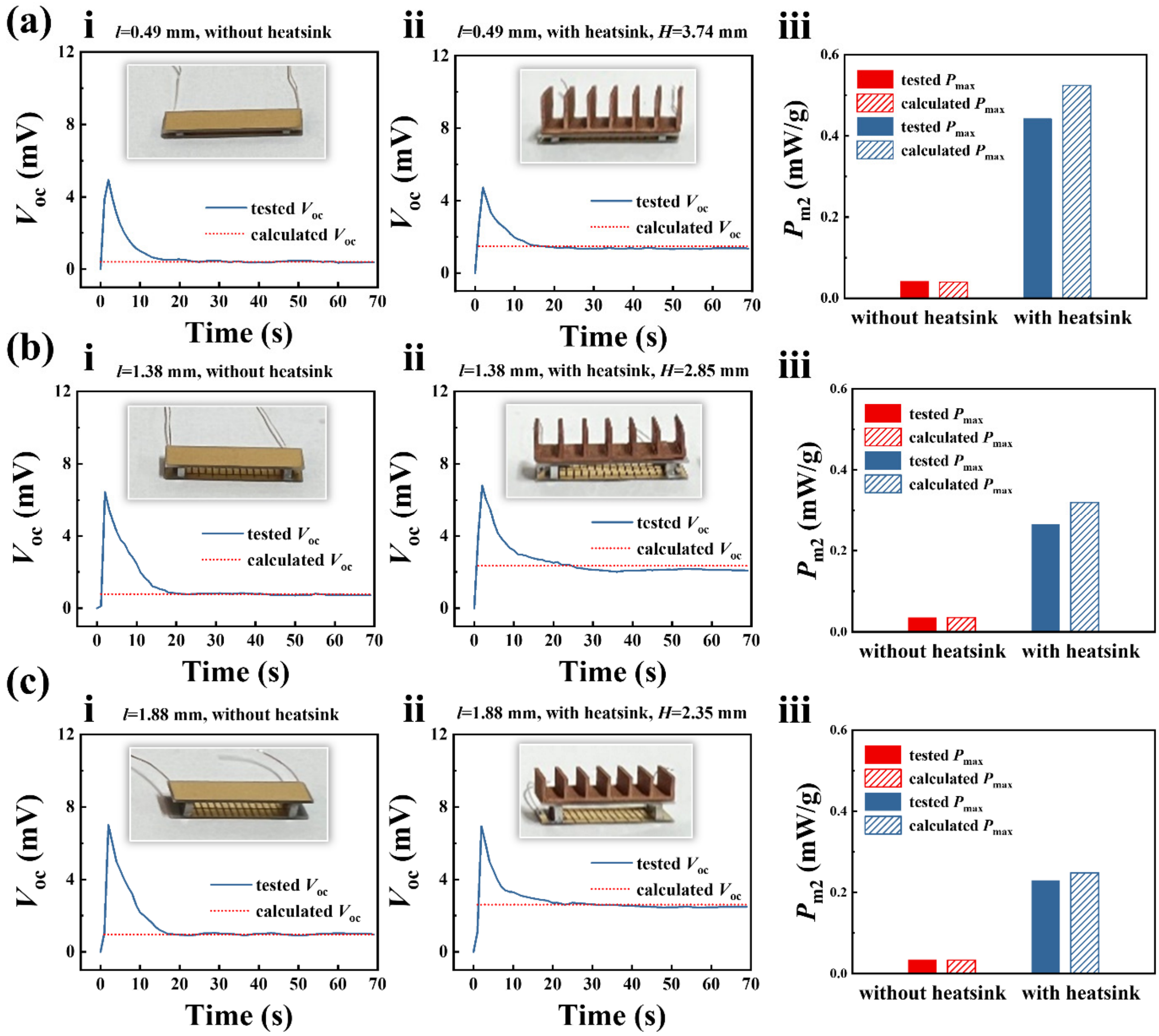

Figure 6. Open-circuit voltage and maximum power density of per unit mass (P_{m2}) of micro-TEGs with different leg heights: (**a**) l = 0.49 mm, (**b**) l = 1.38 mm, (**c**) l = 1.88 mm.

4. Conclusions

In this work, we optimized the design and integrated manufacturing of a wearable micro-thermoelectric generator in a height-confined space. The effects of geometric parameters of thermoelectric generator (TEG) on the number of fins and fin height are systematically studied by numerical simulation. The optimal number of fins to obtain the highest equivalent convective heat transfer coefficient was determined under different fin heights. Our findings reveal that the geometric size of the device has a negligible effect on the heat dissipation capacity of the heat sink, and the optimal number of fins decreases gradually as the fin height increases.

Moreover, a co-design of TEG and fin topological structure was performed to examine the influence of the ratio of leg height to fin height (l/H), leg width (w), and number of thermoelectric leg pairs (N) on the maximum output power density per unit area (P_{m1}), and the maximum output power density per unit mass (P_{m2}) of the device. Notably, when N = 16, w = 0.3 mm, l/H = 2.5 (i.e., l = 3.57 mm and H = 1.43 mm), and P_{m1} reaches the maximum value of 30.5 μW/cm^2; When N = 2, l/H = 0.25 and w = 0.3 mm, P_{m2} reaches a maximum value of 5.12 mW/g. To verify the simulation results, we have fabricated micro-TEGs and measured the open-circuit voltages of TEGs with different thermoelectric leg heights (l = 0.49 mm, l = 1.38 mm, and l = 1.88 mm). The measured values were consistent with the simulated values. Additionally, we found that P_{m2} reached a maximum value of 0.44 mW/g when N = 2, l = 0.49 mm, H = 3.74 mm, and w = 0.85 mm.

Overall, our study provides insights into the optimal design of wearable micro thermoelectric generators working in a height-confined space and highlights the importance of co-designing TEGs and fin topological structures for optimizing their performance. Additionally, future improvements in material properties and the development of advanced technological means will result in less restrictive optimization strategies.

Supplementary Materials: The following supporting information can be downloaded at: https://www.mdpi.com/article/10.3390/app13106156/s1, Figure S1: Temperature dependent properties of p-type $Bi_{0.4}Sb_{1.6}Te_3$ and n-type $Bi_2Se_{0.2}Te_{2.8}$ thermoelectric materials: (a) absolute value of Seebeck coefficient; (b) electrical conductivity; (c) thermal conductivity; Figure S2: The manufacturing process flow chart of the micro device; Figure S3: The relationship among the convective heat transfer coefficient per unit area (h_a), fin height (H) and number of fins under different temperature difference (θ) between fin base and the ambient: (a) θ = 4 K, (b) θ = 5 K, (c) θ = 6 K, (d) θ = 7 K, and (e) θ = 8 K; Figure S4: The relationship among the equivalent convective heat transfer coefficient (h_{eff}), fin height (H) and number of fins under different temperature difference (θ) between fin base and the ambient: (a) θ = 4 K, (b) θ = 5 K, (c) θ = 6 K, (d) θ = 7 K, and (e) θ = 8 K; Figure S5: The relationship among the temperature difference between the two ends of the device (ΔT), the ratio of leg height to fin height (l/H), leg width (w) with different number of leg pairs: (a) 2, (b) 4, (c) 8, (d) 16, and (e) 32.

Author Contributions: K.T. and D.Y. contributed equally to this work. Conceptualization, X.T. and Q.Z.; simulation, K.T., Y.X. and K.H.; investigation, K.T. and J.W.; writing—original draft preparation, K.T.; writing—review and editing, K.T. and D.Y.; supervision, D.Y. and Y.Y.; project administration, X.T. All authors have read and agreed to the published version of the manuscript.

Funding: This work was financially supported by the National Natural Science Foundation of China (52202289), the International Postdoctoral Exchange Fellowship Program (PC2022044), and the National Key Research and Development Program of China (2019YFA0704900).

Institutional Review Board Statement: Not applicable.

Informed Consent Statement: Not applicable.

Data Availability Statement: Data available on request due to restrictions. The data presented in this study are available on request from the corresponding author. The data are not publicly available.

Conflicts of Interest: There are no conflict of interest to declare.

References

1. Liu, Y.; Pharr, M.; Salvatore, G.A. Lab-on-Skin: A Review of Flexible and Stretchable Electronics for Wearable Health Monitoring. *ACS Nano* **2017**, *11*, 9614–9635. [CrossRef] [PubMed]
2. Mathew, A.A.; Chandrasekhar, A.; Vivekanandan, S. A Review on Real-Time Implantable and Wearable Health Monitoring Sensors Based on Triboelectric Nanogenerator Approach. *Nano Energy* **2021**, *80*, 105566. [CrossRef]
3. Khan, Y.; Ostfeld, A.E.; Lochner, C.M.; Pierre, A.; Arias, A.C. Monitoring of Vital Signs with Flexible and Wearable Medical Devices. *Adv. Mater.* **2016**, *28*, 4373–4395. [CrossRef]
4. Wang, L.; Jiang, K.; Shen, G. Wearable, Implantable, and Interventional Medical Devices Based on Smart Electronic Skins. *Adv. Mater. Technol.* **2021**, *6*, 2100107. [CrossRef]
5. Koydemir, H.C.; Ozcan, A. Wearable and Implantable Sensors for Biomedical Applications. *Annu. Rev. Anal. Chem.* **2018**, *11*, 127–146. [CrossRef] [PubMed]
6. Yang, G.; Xie, L.; Mantysalo, M.; Zhou, X.; Pang, Z.; Xu, L.D.; Kao-Walter, S.; Chen, Q.; Zheng, L.-R. A Health-IoT Platform Based on the Integration of Intelligent Packaging, Unobtrusive Bio-Sensor, and Intelligent Medicine Box. *IEEE Trans. Ind. Inf.* **2014**, *10*, 2180–2191. [CrossRef]
7. John Dian, F.; Vahidnia, R.; Rahmati, A. Wearables and the Internet of Things (IoT), Applications, Opportunities, and Challenges: A Survey. *IEEE Access* **2020**, *8*, 69200–69211. [CrossRef]
8. Wang, Y.; Wang, L.; Yang, T.; Li, X.; Zang, X.; Zhu, M.; Wang, K.; Wu, D.; Zhu, H. Wearable and Highly Sensitive Graphene Strain Sensors for Human Motion Monitoring. *Adv. Funct. Mater.* **2014**, *24*, 4666–4670. [CrossRef]
9. Trung, T.Q.; Ramasundaram, S.; Hwang, B.-U.; Lee, N.-E. An All-Elastomeric Transparent and Stretchable Temperature Sensor for Body-Attachable Wearable Electronics. *Adv. Mater.* **2016**, *28*, 502–509. [CrossRef]
10. Peng, B.; Zhao, F.; Ping, J.; Ying, Y. Recent Advances in Nanomaterial-Enabled Wearable Sensors: Material Synthesis, Sensor Design, and Personal Health Monitoring. *Small* **2020**, *16*, 2002681. [CrossRef]

11. Brunelli, D.; Benini, L.; Moser, C.; Thiele, L. An Efficient Solar Energy Harvester for Wireless Sensor Nodes. In Proceedings of the Proceedings—Design, Automation and Test in Europe, DATE, Munich Germany, 10–14 March 2008; pp. 104–109.
12. Zhao, J.; Ghannam, R.; Htet, K.O.; Liu, Y.; Law, M.; Roy, V.A.L.; Michel, B.; Imran, M.A.; Heidari, H. Self-Powered Implantable Medical Devices: Photovoltaic Energy Harvesting Review. *Adv. Healthc. Mater.* **2020**, *9*, 2000779. [CrossRef] [PubMed]
13. Aslam, A.; Mehmood, U.; Arshad, M.H.; Ishfaq, A.; Zaheer, J.; Ul Haq Khan, A.; Sufyan, M. Dye-Sensitized Solar Cells (DSSCs) as a Potential Photovoltaic Technology for the Self-Powered Internet of Things (IoTs) Applications. *Sol. Energy* **2020**, *207*, 874–892. [CrossRef]
14. Shi, Y.; Wang, Y.; Deng, Y.; Gao, H.; Lin, Z.; Zhu, W.; Ye, H. A Novel Self-Powered Wireless Temperature Sensor Based on Thermoelectric Generators. *Energy Convers. Manag.* **2014**, *80*, 110–116. [CrossRef]
15. Zhao, Y.; Dyck, J.S.; Hernandez, B.M.; Burda, C. Enhancing Thermoelectric Performance of Ternary Nanocrystals through Adjusting Carrier Concentration. *J. Am. Chem. Soc.* **2010**, *132*, 4982–4983. [CrossRef] [PubMed]
16. Harb, A. Energy Harvesting: State-of-the-Art. *Renew. Energy* **2011**, *36*, 2641–2654. [CrossRef]
17. Lee, J.; Choi, B. Development of a Piezoelectric Energy Harvesting System for Implementing Wireless Sensors on the Tires. *Energy Convers. Manag.* **2014**, *78*, 32–38. [CrossRef]
18. Chen, J.; Wang, Z.L. Reviving Vibration Energy Harvesting and Self-Powered Sensing by a Triboelectric Nanogenerator. *Joule* **2017**, *1*, 480–521. [CrossRef]
19. Bell, L.E. Cooling, Heating, Generating Power, and Recovering Waste Heat with Thermoelectric Systems. *Science* **2008**, *321*, 1457–1461. [CrossRef]
20. Pourkiaei, S.M.; Ahmadi, M.H.; Sadeghzadeh, M.; Moosavi, S.; Pourfayaz, F.; Chen, L.; Pour Yazdi, M.A.; Kumar, R. Thermoelectric Cooler and Thermoelectric Generator Devices: A Review of Present and Potential Applications, Modeling and Materials. *Energy* **2019**, *186*, 115849. [CrossRef]
21. Zoui, M.A.; Bentouba, S.; Stocholm, J.G.; Bourouis, M. A Review on Thermoelectric Generators: Progress and Applications. *Energies* **2020**, *13*, 3606. [CrossRef]
22. Misra, V.; Bozkurt, A.; Calhoun, B.; Jackson, T.; Jur, J.; Lach, J.; Lee, B.; Muth, J.; Oralkan, O.; Ozturk, M.; et al. Flexible Technologies for Self-Powered Wearable Health and Environmental Sensing. *Proc. IEEE* **2015**, *103*, 665–681. [CrossRef]
23. Zhang, F.; Zang, Y.; Huang, D.; Di, C.; Zhu, D. Flexible and Self-Powered Temperature–Pressure Dual-Parameter Sensors Using Microstructure-Frame-Supported Organic Thermoelectric Materials. *Nat. Commun.* **2015**, *6*, 8356. [CrossRef] [PubMed]
24. Yuan, J.; Zhu, R. A Fully Self-Powered Wearable Monitoring System with Systematically Optimized Flexible Thermoelectric Generator. *Appl. Energy* **2020**, *271*, 115250. [CrossRef]
25. Wang, Y.; Shi, Y.; Mei, D.; Chen, Z. Wearable Thermoelectric Generator to Harvest Body Heat for Powering a Miniaturized Accelerometer. *Appl. Energy* **2018**, *215*, 690–698. [CrossRef]
26. Torfs, T.; Leonov, V.; Yazicioglu, R.F.; Merken, P.; Van Hoof, C.; Vullers, R.J.M.; Gyselinckx, B. Wearable Autonomous Wireless Electro-Encephalography System Fully Powered by Human Body Heat. In Proceedings of the 2008 IEEE Sensors, Lecce, Italy, 26–29 October 2008; IEEE: Piscataway, NJ, USA, 2008; pp. 1269–1272.
27. Mohsen, S.; Zekry, A.; Youssef, K.; Abouelatta, M. A Self-Powered Wearable Wireless Sensor System Powered by a Hybrid Energy Harvester for Healthcare Applications. *Wirel. Pers. Commun.* **2021**, *116*, 3143–3164. [CrossRef]
28. Martínez, A.; Vián, J.G.; Astrain, D.; Rodríguez, A.; Berrio, I. Optimization of the Heat Exchangers of a Thermoelectric Generation System. *J. Electron. Mater.* **2010**, *39*, 1463–1468. [CrossRef]
29. Meng, F.; Chen, L.; Sun, F.; Yang, B. Thermoelectric Power Generation Driven by Blast Furnace Slag Flushing Water. *Energy* **2014**, *66*, 965–972. [CrossRef]
30. Benn, S.P.; Poplaski, L.M.; Faghri, A.; Bergman, T.L. Analysis of Thermosyphon/Heat Pipe Integration for Feasibility of Dry Cooling for Thermoelectric Power Generation. *Appl. Therm. Eng.* **2016**, *104*, 358–374. [CrossRef]
31. Date, A.; Date, A.; Dixon, C.; Akbarzadeh, A. Theoretical and Experimental Study on Heat Pipe Cooled Thermoelectric Generators with Water Heating Using Concentrated Solar Thermal Energy. *Sol. Energy* **2014**, *105*, 656–668. [CrossRef]
32. Fan, W.; An, Z.; Liu, F.; Gao, Z.; Zhang, M.; Fu, C.; Zhu, T.; Liu, Q.; Zhao, X. High-Performance Stretchable Thermoelectric Generator for Self-Powered Wearable Electronics. *Adv. Sci.* **2023**, *10*, 2206397. [CrossRef]
33. Chen, W.-H.; Wang, C.-M.; Huat Saw, L.; Hoang, A.T.; Bandala, A.A. Performance Evaluation and Improvement of Thermoelectric Generators (TEG): Fin Installation and Compromise Optimization. *Energy Convers. Manag.* **2021**, *250*, 114858. [CrossRef]
34. Garud, K.S.; Seo, J.-H.; Patil, M.S.; Bang, Y.-M.; Pyo, Y.-D.; Cho, C.-P.; Lee, M.-Y. Thermal–Electrical–Structural Performances of Hot Heat Exchanger with Different Internal Fins of Thermoelectric Generator for Low Power Generation Application. *J. Anal. Calorim.* **2021**, *143*, 387–419. [CrossRef]
35. Bouknadel, A.; Rah, I.; El Omari, H.; El Omari, H. Comparative Study of Fin Geometries for Heat Sinks in Natural Convection. In Proceedings of the 2014 International Renewable and Sustainable Energy Conference (IRSEC), Ouarzazate, Morocco, 17–19 October 2014; IEEE: Piscataway, NJ, USA, 2014; pp. 723–728.
36. Kim, T.Y.; Lee, S.; Lee, J. Fabrication of Thermoelectric Modules and Heat Transfer Analysis on Internal Plate Fin Structures of a Thermoelectric Generator. *Energy Convers. Manag.* **2016**, *124*, 470–479. [CrossRef]
37. Quan, R.; Li, Y.; Li, T.; Chang, Y.; Yan, H. Numerical and Experimental Study on Performance of a Low-Backpressure Polyhedral Thermoelectric Generator for Waste Heat Recovery. *J. Therm. Sci.* **2023**, *32*, 109–124. [CrossRef]

38. Antonova, E.E.; Looman, D.C. Finite Elements for Thermoelectric Device Analysis in ANSYS. In Proceedings of the 24th International Conference on Thermoelectrics, Clemson, SC, USA, 19–23 June 2005; IEEE: Piscataway, NJ, USA, 2005; pp. 215–218.
39. Jia, X.-D.; Wang, Y.-J.; Gao, Y.-W. Numerical Simulation of Thermoelectric Performance of Linear-Shaped Thermoelectric Generators under Transient Heat Supply. *Energy* **2017**, *130*, 276–285. [CrossRef]
40. Luo, X.; Xiong, W.; Cheng, T.; Liu, S. Design and Optimization of Horizontally-Located Plate Fin Heat Sink for High Power LED Street Lamps. In Proceedings of the 2009 59th Electronic Components and Technology Conference, San Diego, CA, USA, 26–29 May 2009; IEEE: Piscataway, NJ, USA, 2009; pp. 854–859.
41. Incropera, F.P.; DeWitt, D.P. *Fundamentals of Heat and Mass Transfer*; Wiley: New York, NY, USA, 1985.
42. Bar-Cohen, A.; Rohsenow, W.M. Thermally Optimum Spacing of Vertical, Natural Convection Cooled, Parallel Plates. *J. Heat Transf.* **1984**, *106*, 116–123. [CrossRef]
43. Tang, K.; Yang, D.; Hu, K.; Li, J.; Wang, J.; Wu, Y.; Ming, T.; Yan, Y.; Zhang, Q.; Uher, C.; et al. Multi-Factor Roadmap for Designing Wearable Micro Thermoelectric Generators. *Energy Convers. Manag.* **2023**, *280*, 116819. [CrossRef]
44. Kim, C.S.; Lee, G.S.; Choi, H.; Kim, Y.J.; Yang, H.M.; Lim, S.H.; Lee, S.-G.; Cho, B.J. Structural Design of a Flexible Thermoelectric Power Generator for Wearable Applications. *Appl. Energy* **2018**, *214*, 131–138. [CrossRef]
45. Shi, Y.; Wang, Y.; Mei, D.; Feng, B.; Chen, Z. Design and Fabrication of Wearable Thermoelectric Generator Device for Heat Harvesting. *IEEE Robot. Autom. Lett.* **2018**, *3*, 373–378. [CrossRef]
46. Leonov, V. Thermoelectric Energy Harvesting of Human Body Heat for Wearable Sensors. *IEEE Sens. J.* **2013**, *13*, 2284–2291. [CrossRef]
47. Suarez, F.; Nozariasbmarz, A.; Vashaee, D.; Öztürk, M.C. Designing Thermoelectric Generators for Self-Powered Wearable Electronics. *Energy Environ. Sci.* **2016**, *9*, 2099–2113. [CrossRef]
48. Hong, S.; Gu, Y.; Seo, J.K.; Wang, J.; Liu, P.; Meng, Y.S.; Xu, S.; Chen, R. Wearable Thermoelectrics for Personalized Thermoregulation. *Sci. Adv.* **2019**, *5*, eaaw0536. [CrossRef] [PubMed]